

Theory of Laser-Induced Adiabatic Shaping in Inertial Fusion Implosions: The Relaxation Method

Introduction

In recent years it has been theoretically shown that the stability of inertial fusion implosions can be significantly improved by shaping the entropy inside the shell. The optimum adiabat shape in the shell consists of a profile that is monotonically decreasing from the outer to the inner surface. Large values of the adiabat on the outer shell surface increase the ablation velocity V_a , which follows a power law of the outer-surface adiabat α_{out} ,

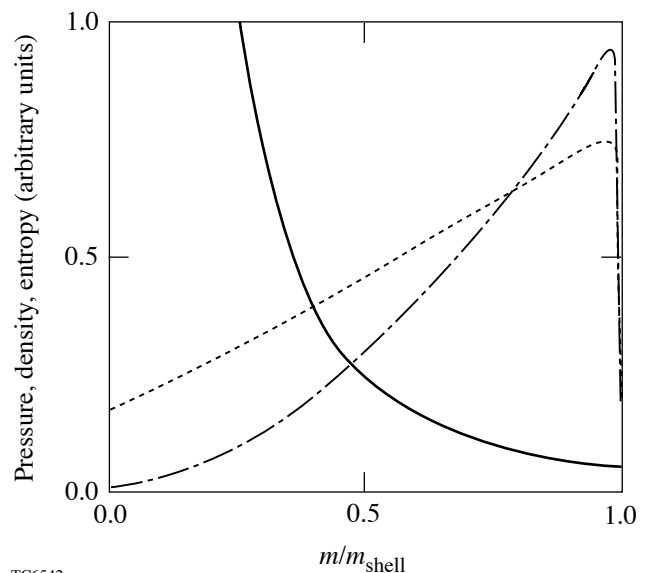
$$V_a \sim \alpha_{out}^{3/5}, \quad (1)$$

while low adiabat values on the inner surface lead to improved ignition conditions and larger burn fraction. A more-detailed history and target design implications of adiabat shaping can be found in the introduction of Ref. 1, which is mostly devoted to the adiabat shape induced by a strong decaying shock. Shaping by a decaying shock^{1,2} requires a very strong prepulse, followed by a low-intensity foot of the main pulse, to launch a strong shock, which decays inside the shell shortly after the prepulse is turned off. The decaying shock (DS) leaves behind a monotonically decreasing adiabat profile, which follows a power law of the mass coordinate

$$\alpha = \alpha_{in} \left(\frac{m_{shell}}{m} \right)^{\Delta_{DS}}, \quad (2)$$

where m is the mass calculated from the outer surface, m_{shell} is the total shell mass, and Δ_{DS} varies between 1.06 and 1.13 depending on the prepulse duration. Two-dimensional simulations² of all-DT, OMEGA-sized capsule implosions have confirmed that DS adiabat targets exhibit significantly reduced Rayleigh–Taylor growth on the ablation surface during the acceleration phase with respect to the flat-adiabat targets. Comparisons between flat- and shaped-adiabat targets are typically carried out by designing the flat- and shaped-adiabat pulses to generate identical adiabats on the inner shell surface.

A different technique aimed at shaping the adiabat is the so-called shaping by relaxation (or RX shaping) described in Ref. 3. The relaxation technique uses a less-energetic prepulse than the DS technique. The RX prepulse is used to launch a shock that may or may not decay inside the shell. In both cases, the prepulse is turned off before the prepulse shock reaches the shell's inner surface. Since the prepulse is followed by a complete power shutoff, the outer portion of the shell expands outward, generating a relaxed density profile, while the prepulse shock travels inside the shell. The prepulse shock is not intended to greatly change the shell adiabat even though it may cause a significant adiabat modification. The main adiabat shaping occurs later in time when the foot of the main pulse starts, driving a strong shock up the relaxed density profile. The main shock first encounters the low-density portion of the relaxed profile, setting it on a very high adiabat. The adiabat develops a monotonically decreasing profile as a result of the increasing pre-shock density. Figure 98.43 shows a plot of the



TC6542

Figure 98.43

Pressure (dashed), density (dot-dashed), and adiabat (solid) profiles generated by a strong shock supported by constant pressure propagating through a relaxed density profile.

pressure, density, and entropy profiles generated by a strong shock propagating through a relaxed density profile. Observe that the adiabat profile is strongly shaped with large values on the outer shell surface and low values on the inner shell surface. To produce a monotonically decreasing adiabat profile, it is important to design the laser pulse so that the prepulse and main shock merge at the inner shell surface. The RX adiabat-shaping technique can be viewed as a two-step process: the prepulse and power shutoff are needed to generate the relaxed density profile, following which the foot of the main pulse shapes the adiabat.

In this article, a detailed hydrodynamic analysis of the relaxed profile generation as well as the shock propagation through these profiles is carried out.

The General Model

The general gasdynamic model governing the hydrodynamic motion of a compressible gas is greatly simplified by adopting a Lagrangian frame of reference where the independent spatial coordinate is the mass. In planar geometry, the mass coordinate is defined as the mass per unit area calculated from the outer shell surface:

$$m = \int_0^{\bar{x}} \rho(\bar{x}', 0) d\bar{x}', \quad (3)$$

where $\rho(\bar{x}, 0)$ is the initial density and \bar{x} is the initial spatial location of the fluid elements.

In this coordinate, the outer shell surface is represented by $\bar{x} = 0$ and $m = 0$. In spherical geometry, Eq. (3) should be replaced by $m = \int_0^{\bar{r}} \bar{r}'^2 \rho(\bar{r}', 0) d\bar{r}'$. For simplicity, we carry out the calculation for the case of an ideal gas with adiabatic index γ and neglect convergence effects on the basis that the adiabat shaping occurs when the inner shell surface has not yet moved and the initial aspect ratio is sufficiently large that the shell can be approximated with a uniform slab.

In the Lagrangian frame and away from the shock front, the planar equations of motion for the shocked material can be written in the following conservative form:

$$\frac{\partial u}{\partial m} - \frac{\partial}{\partial t} \frac{1}{\rho} = 0, \quad (4)$$

$$\frac{\partial u}{\partial t} + \frac{\partial P}{\partial m} = 0, \quad (5)$$

$$p = S(m)\rho^\gamma, \quad (6)$$

where u , P , ρ , and $S(m)$ are the velocity, pressure, density, and entropy, respectively. The function $S(m)$ is referred to as the adiabat and depends exclusively on the Lagrangian coordinate. At the shock front, the physical quantities must satisfy the Hugoniot conditions, which in the strong shock regime can be written in the following simple form:

$$\left[\rho_{\text{ps}} \right]_{m_{\text{sh}}} = \frac{\gamma + 1}{\gamma - 1} \left[\rho_0 \right]_{m_{\text{sh}}}, \quad (7)$$

$$\left[u_{\text{ps}} \right]_{m_{\text{sh}}} = \frac{2}{\gamma - 1} \frac{\dot{m}_{\text{sh}}}{\left[\rho_{\text{ps}} \right]_{m_{\text{sh}}}}, \quad (8)$$

$$\dot{m}_{\text{sh}} = \sqrt{\frac{(\gamma - 1)}{2} \left[P_{\text{ps}} \rho_{\text{ps}} \right]_{m_{\text{sh}}}}, \quad (9)$$

where P_{ps} represents the post-shock pressure, ρ_{ps} is the post-shock density, u_{ps} is the post-shock velocity, and ρ_0 is the initial unshocked density. Here, m_{sh} is the mass coordinate corresponding to the shock location. More details on the Lagrangian model used here can be found in Ref. 1.

The Generation of the Relaxed Profiles

When a square laser prepulse precedes the main laser pulse, a pressure pulse is applied to the shell's outer surface, launching a uniform shock followed by a rarefaction wave, which causes a relaxation of the pressure and density profiles. Since the leading edge of the rarefaction wave travels faster than the shock, it eventually catches the shock unless the shock reaches the inner shell surface before interacting with the rarefaction wave. Two different relaxed profiles are generated depending on whether or not the rarefaction leading edge catches the prepulse shock inside the shell. If the shock and rarefaction do not merge in the shell, the resulting relaxed profiles are said to be of the "first kind" while merging leads to relaxed profiles of the "second kind."

It is convenient to define with subscript p the prepulse quantities, P_p , ρ_p , S_p , a_p , and u_p , representing the induced pressure, compressed density, adiabat, sound speed, and flow velocity while the uniform laser prepulse of duration Δt_p is applied. Using the prepulse quantities, we define the following set of dimensionless quantities and coordinates:

$$\hat{\rho} \equiv \frac{\rho}{\rho_p}, \quad \hat{P} \equiv \frac{P}{P_p}, \quad \hat{u} \equiv \frac{u}{a_p}, \quad (10)$$

$$\hat{S} = \frac{S}{S_p}, \quad z = \frac{m}{m_*}, \quad \tau = \frac{t}{\Delta t_*}, \quad (11)$$

where

$$\Delta t_* = \frac{\Delta t_p}{\sqrt{2\gamma/(\gamma-1)} - 1}, \quad (12)$$

$$m_* = \Delta t_* \rho_p a_p = \Delta t_* \sqrt{\gamma P_p \rho_p}. \quad (13)$$

Here Δt_* is the travel time of the rarefaction wave before catching the shock, and m_* is the areal density undertaken by the rarefaction wave's leading edge before catching the prepulse shock. Furthermore, $\tau = 0$ is defined as the time when the laser prepulse is terminated and the rarefaction wave is launched. It follows that $\tau = 1$ represents the shock–rarefaction interaction time.

These dimensionless variables can be used to rewrite the Lagrangian equations of motion in the convenient form

$$\frac{\partial \hat{u}}{\partial z} = \frac{\partial \hat{\rho}^{-1}}{\partial \tau}, \quad (14)$$

$$\gamma \frac{\partial \hat{u}}{\partial \tau} = -\frac{\partial \hat{P}}{\partial z}, \quad (15)$$

$$\hat{P} = \hat{S}(z) \hat{\rho}^\gamma. \quad (16)$$

Observe that Eqs. (14)–(16) can be combined into the following single equation:

$$\gamma \frac{\partial^2}{\partial \tau^2} \frac{1}{\hat{\rho}} + \frac{\partial^2}{\partial z^2} \hat{S}(z) \hat{\rho}^\gamma = 0, \quad (17)$$

which can be solved for $\hat{\rho}$ once \hat{S} is known. There is no general solution of the equations of motion after the rarefaction wave is launched; however, one can consider two limiting cases resulting in two different relaxed profiles. The first is the case when the rarefaction wave catches the shock at the

shell's rear surface. This case is characterized by values of $m_* = m_{\text{shell}}$. The second is the case when the rarefaction wave quickly catches the shock near the outer surface, causing the shock to decay throughout most of the shell. This case requires a small m_* satisfying $m_* < m_{\text{shell}}$. We will consider these two cases separately.

1. Relaxed Profiles of the First Kind: Rarefaction and Shock Merge at the Rear Surface of the Shell: $m_* = m_{\text{shell}}$

In this case, the relaxed density and pressure profiles are the ones generated by the rarefaction wave, whose functional forms can be obtained from Ref. 1 or from most textbooks on compressible flow. In the mass coordinate, the density profile can be written in the following simple form:

$$\rho(z < \tau) = \rho_p \left(\frac{z}{\tau} \right)^{\frac{2}{\gamma+1}} = \rho_p \left(\frac{m}{m_{\text{rf}}} \right)^{\frac{2}{\gamma+1}}, \quad (18)$$

where $m_{\text{rf}} = a_p \rho_p t$ represents the trajectory of the rarefaction wave's leading edge. For $z > \tau$, the density is uniform and equal to the post-shock density $\rho = \rho_p$.

2. Relaxed Profiles of the Second Kind: Rarefaction Catches the Shock Inside the Shell: $m_* < m_{\text{shell}}$

In this case, the derivation of the relaxed profiles is significantly more complicated since there is no exact solution of the equations of motion after the rarefaction wave catches the prepulse shock. After the rarefaction wave reaches the shock at $z = 1$, the latter decays, leaving behind a relaxed profile with two distinct spatial shapes in the regions $0 < m < m_*$ and $m_* < m < m_s^p$, where m_s^p is the location of the prepulse shock. In the dimensionless variable $z = m/m_*$, those two regions are $0 < z < 1$ and $1 < z < z_s^p$, where $z_s^p \equiv m_s^p/m_*$.

a. The region $z < 1$. One could speculate that the profiles in the region $0 < z < 1$ have a similar shape to the ones generated by the rarefaction wave, $\rho \sim z^{2/\gamma+1}$; however, this assumption does not take into account a second profile relaxation occurring when a sound wave travels backward down the rarefaction-wave profile right after the rarefaction wave catches the shock. The solution in the regions $0 < z < 1$ must satisfy Eq. (17) and the boundary conditions at $z = 0$ and $z = 1$. At $z = 0$, the vacuum boundary condition requires that $\rho(z = 0) = 0$. At $z = 1$, both the pressure and its gradient must be continuous to prevent separation of the continuous medium requiring that

$$P(z = 1^-, \tau) = P(z = 1^+, \tau), \quad (19)$$

$$\frac{dP}{dz}(z = 1^-, \tau) = \frac{dP}{dz}(z = 1^+, \tau).$$

It would be unrealistic to hope that a simple power law in z would exactly satisfy the equations of motion and the boundary conditions; however, one could attempt to look for an approximate solution behaving as a power law of the mass coordinate

$$\hat{\rho} \approx \bar{\rho}(\tau)z^\alpha, \quad (20)$$

which, by construction, satisfies the boundary conditions at $z = 0$. Substituting Eq. (20) into Eq. (17) with $\hat{S} = 1$ leads to the following two conditions:

$$\frac{d^2}{d\tau^2} \frac{1}{\bar{\rho}} + \alpha(\alpha\gamma - 1)\bar{\rho}^\gamma \approx 0, \quad (21)$$

$$F_1(\alpha) \equiv \frac{\alpha(\gamma + 1)}{2} \approx 1. \quad (22)$$

Note that the symbol \approx has been used to indicate that the function (20) is meant to represent an approximate rather than an exact solution. To solve Eq. (21), one needs two initial conditions for $\bar{\rho}$ and $d\bar{\rho}/d\tau$ at $\tau = 1^+$ just after the rarefaction wave interacts with the shock. While the initial condition for the density at $z = 1$ is trivial,

$$\bar{\rho}(\tau = 1^+) = 1, \quad (23)$$

the condition on the time derivative at $\tau = 1^+$ is rather complicated. The exact derivation of $\hat{\rho}'(1, 1)$ is described in Ref. 1 and leads to Eq. (56) of Ref. 1, which reads as

$$\left[\frac{d\bar{\rho}}{d\tau} \right]_{\tau=1^+} = - \frac{6/(\gamma + 1)}{\frac{3}{2} + \sqrt{\frac{\gamma}{2(\gamma - 1)}} + \sqrt{\frac{\gamma - 1}{2\gamma}}}. \quad (24)$$

It is worth mentioning that the initial condition on the density spatial profile at $\tau = 1$ requires that the function $\hat{\rho}(\tau = 1, z) \approx \bar{\rho}(1)z^\alpha$ reproduces the rarefaction-wave solution

$\hat{\rho}(1, z) = z^{2/\gamma+1}$, thus requiring that the power index α satisfies $\alpha - 2/(\gamma + 1) \approx 0$. This condition is identical to Eq. (22) and does not represent an additional condition. Note that a simple analytical solution of Eq. (21) is the following power law:

$$\bar{\rho}(\tau) = \left[\frac{2(\gamma - 1)}{\alpha(\gamma + 1)^2(\alpha\gamma - 1)} \right]^{\frac{1}{\gamma+1}} \frac{1}{\tau^{\frac{2}{\gamma+1}}}. \quad (25)$$

Equation (25) satisfies the initial conditions (23) and (24) only if the following conditions are met:

$$F_2(\alpha) \equiv \left[\frac{2(\gamma - 1)}{\alpha(\gamma + 1)^2(\alpha\gamma - 1)} \right]^{\frac{1}{\gamma+1}} \approx 1, \quad (26)$$

$$F_3(\alpha) \equiv \frac{1}{3} \left[\frac{2(\gamma - 1)}{\alpha(\gamma + 1)^2(\alpha\gamma - 1)} \right]^{\frac{1}{\gamma+1}} \times \left(\frac{3}{2} + \sqrt{\frac{\gamma}{2(\gamma - 1)}} + \sqrt{\frac{\gamma - 1}{2\gamma}} \right) \approx 1. \quad (27)$$

To test Eq. (20) against the remaining boundary conditions (19) at $z = 1$, one needs to determine the solution for $z > 1$ carried out in the next section. In any case, the condition (22) implies that $\alpha \approx 2/(\gamma + 1)$, indicating that the density profile shape is little changed by the second relaxation occurring after the shock–rarefaction merging.

b. The region $1 < z < z_s^P$. As mentioned earlier, the shock decays for $z > 1$, $\tau > 1$. The entropy profile left behind by the decaying shock is calculated in Ref. 1 and approximately follows a power law of the Lagrangian coordinate m (or z):

$$\hat{S}(z) \approx \frac{1}{z^\delta}, \quad (28)$$

where $\delta \approx 1.31$ when the effects of ablation are neglected and the spatial range is limited to $z < 10$. Typically, the range $1 < z < 10$ includes most (if not all) of the ICF RX target

designs for both OMEGA-like as well as NIF-like capsules. However, if $z > 10$, the shock decay becomes self-similar and the power-law index asymptotically approaches the value $\delta \approx 1.275$. The residual ablation pressure leads to a somewhat slower decay and can be accounted for through a lower δ (approximately 17% lower) as indicated in Ref. 1. In the self-similar solution, the density is a function of the coordinate

$$\xi = \frac{z}{z_s^p}, \quad (29)$$

where z_s^p is the trajectory of the decaying shock, satisfying the Hugoniot condition

$$\dot{z}_s^p = \sqrt{\frac{\gamma-1}{2\gamma} \frac{1}{(z_s^p)^\delta}}. \quad (30)$$

Equation (30) can be easily integrated with the initial condition $z_s^p(1) = 1$, leading to the following form of the decelerating shock trajectory:

$$z_s^p(\tau) = \left[1 + \left(1 + \frac{\delta}{2} \right) \sqrt{\frac{\gamma-1}{2\gamma}} (\tau-1) \right]^{\frac{2}{2+\delta}}. \quad (31)$$

The density $\hat{\rho}(\xi)$ does not follow a power law. Instead it must satisfy a complicated second-order differential equation derived by substituting Eqs. (16) and (28) into (17), leading to

$$\xi \frac{d}{d\xi} \left[1 + \frac{\delta}{2} + \xi \frac{d}{d\xi} \right] \frac{1}{\hat{\rho}} + \frac{2}{\gamma-1} \frac{d^2}{d\xi^2} \frac{\hat{\rho}^\gamma}{\xi^\delta} = 0. \quad (32)$$

Equation (32) cannot be exactly integrated; however, one can again attempt to look for an approximate solution in the form of a power law of the self-similar coordinate

$$\hat{\rho} \approx \xi^\mu, \quad (33)$$

which approximately satisfies not only Eq. (32) but also the boundary by conditions at $z = 1$ [Eqs. (19)] and at the shock front $z = z_s^p$. In order for the simple power law (33) to approximate the solution of Eq. (32), the power index μ must satisfy the following conditions obtained upon substitution of (33)

into (32):

$$G_1(\mu) \equiv \frac{\mu(\gamma+1)}{\delta+2} \approx 1, \quad (34)$$

$$G_2(\mu) \equiv \frac{\mu(\gamma-1) \left(1 + \frac{\delta}{2} - \mu \right)}{2(\mu\gamma - \delta)(\mu\gamma - \delta - 1)} \approx 1. \quad (35)$$

The boundary conditions at the shock front are provided by the Hugoniot conditions that determine $\hat{\rho}$ and $d\hat{\rho}/d\xi$ at $\xi = 1$. Note that the density gradient can be obtained from Eqs. (35b) and (36) of Ref. 1 for $\xi = 1$, yielding the following condition:

$$\frac{d\hat{\rho}}{d\xi}(\xi=1) = \frac{3\delta}{\gamma+1}. \quad (36)$$

While the Hugoniot condition on the density $\hat{\rho}(1) = 1$ is trivially satisfied by $\hat{\rho} = \xi^\mu$, the condition on $d\hat{\rho}/d\xi$ requires that

$$G_3(\mu) \equiv \frac{\mu(\gamma+1)}{3\delta} \approx 1. \quad (37)$$

The next step is to verify that Eq. (33) used for $z > 1$ satisfies Eqs. (19) at $z = 1$. Since the entropy is continuous at $z = 1$, the first of Eq. (19) requires that the density be continuous; therefore $\hat{\rho}(z=1^-, \tau) \approx \hat{\rho}(z=1^+, \tau)$, yielding

$$\bar{\rho}(\tau) \approx \frac{1}{[z_s^p(\tau)]^\mu}. \quad (38)$$

Then, using the continuity of the density and Eqs. (28) and (33) into the second of Eq. (19), one finds the condition

$$H(\alpha, \mu) \equiv \frac{\gamma\alpha + \delta}{\gamma\mu} \approx 1. \quad (39)$$

The last step is to find the two power indices α and μ in such a way that all the conditions [Eqs. (22), (26), (27), (34), (35), (37), and (39)] are met and that Eq. (38) is approximately satisfied for any time τ limited by $z_s^p(\tau) \leq 10$ representing the range of interest for ICF capsule design.

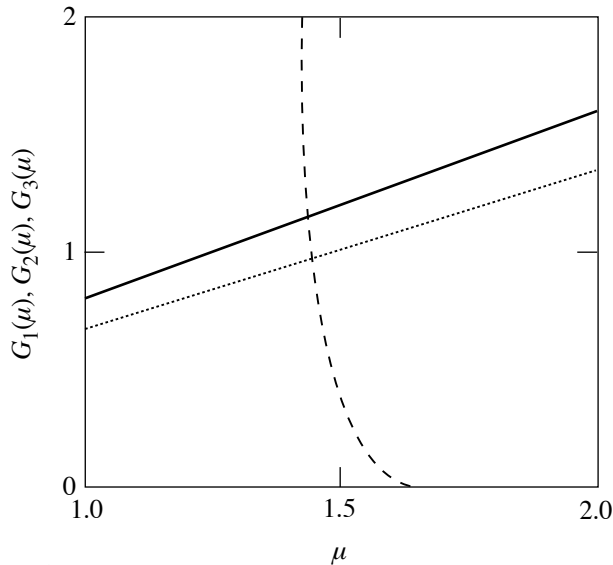
c. **Determination of the power indices.** The power indices α and τ can be determined by plotting the conditions

$$G_1(\mu) \approx 1, \quad G_2(\mu) \approx 1, \quad G_3(\mu) \approx 1, \quad (40)$$

$$F_1(\alpha) \approx 1, \quad F_2(\alpha) \approx 1, \quad F_3(\alpha) \approx 1, \quad (41)$$

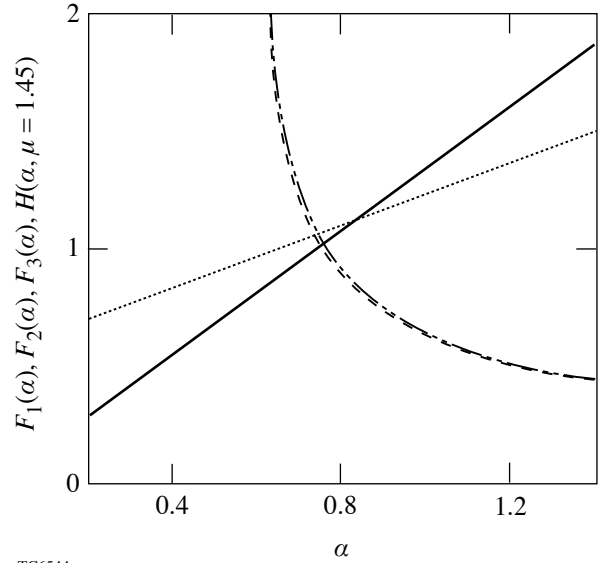
$$H(\alpha, \mu) \approx 1, \quad (42)$$

and determining α and μ so that all such conditions are approximately satisfied. Figure 98.44 shows the plot of three functions G_1 , G_2 , and G_3 that depends exclusively on the power index μ for a given $\gamma = 5/3$ and $\delta \approx 1.315$. Observe that all the G -functions exhibit a zero near $\mu \approx 1.45$, which can be considered as an approximate solution of all the Eqs. (40). After determining μ , the F -functions are plotted together with the function H versus the parameter α (Fig. 98.45), clearly indicating that $\alpha \approx 0.75$ is an approximate solution of all Eqs. (41) and (42). The last step is to verify that Eq. (38) is approximately satisfied for any time τ and for $z_s^p \leq 10$. First, it is easily found from Eq. (31) that the condition $z_s^p \leq 10$ requires $\tau \leq 61$. Second, we plot both sides of Eq. (38) versus time for $\tau \leq 61$ (Fig. 98.46) and realize that both functions are approximately equal over the range of interesting times.



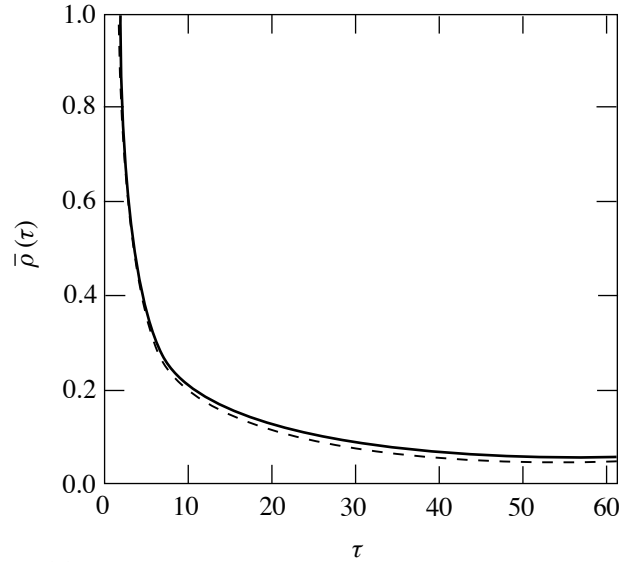
TC6543

Figure 98.44
The functions $G_1(\mu)$ (solid), $G_2(\mu)$ (dashed), and $G_3(\mu)$ (dotted) are all approximately equal to 1 at $\mu = 1.45$.



TC6544

Figure 98.45
The functions $F_1(\alpha)$ (solid), $F_2(\alpha)$ (dashed), $F_3(\alpha)$ (dashed–double-dotted), and $H(\alpha, \mu = 1.45)$ (dotted) are all approximately equal to 1 at $\alpha = 0.75$.



TC6545

Figure 98.46
The analytic solution of Eqs. (21), (23), and (24) for $\bar{\rho}(\tau)$ given by Eq. (25) (solid) is compared to the approximate solution for $\bar{\rho}(\tau)$ given by Eq. (38) using $\mu = 1.45$ (dashed). The plot indicates good agreement between the two functional forms of $\bar{\rho}(\tau)$.

In summary, all the equations of motions and boundary conditions for $\tau > 1$ are approximately satisfied by simple power laws of the Lagrangian coordinate z , leading to the following solutions for $\gamma = 5/3$:

$$\rho(z < 1) \approx \rho_p \left(\frac{z}{\tau} \right)^{3/4} = \rho_p \left(\frac{m}{m_{\text{rf}}} \right)^{3/4}, \quad (43)$$

$$\rho(1 < z < z_s^p) \approx \rho_p \left(\frac{z}{z_s^p(\tau)} \right)^{1.45} = \rho_p \left(\frac{m}{m_s^p(\tau)} \right)^{1.45}, \quad (44)$$

where m_s^p represents the trajectory of the prepulse shock $m_s^p = z_s^p m_*$ and $m_{\text{rf}} = a_p \rho_p t$. Here $t = 0$ represents the end of the prepulse. This concludes the calculation of the relaxed profiles. The next step is to determine the adiabat shape induced by the main shock propagating through the relaxed profiles of the first and second kind described by Eqs. (18) and [(43), (44)], respectively.

Main Shock Propagation Through the Relaxed Profiles

Before the prepulse shock reaches the rear surface, the main shock is launched by the foot of the main laser pulse and supported by the applied pressure P_f , which is assumed constant during the main shock propagation. The adiabat shaping occurs when the main shock travels up the relaxed density profile, shocking material with increasing density to lower and lower adiabats. The main shock is typically a strong shock in the sense that the ratio of pressures across the shock front is much larger than unity. Using the strong-shock form of the Hugoniot relations leads to a great simplification of the hydrodynamic analysis and is often accurate for the main shock propagation. However, it is important to emphasize that some of the strong-shock Hugoniot relations are accurately satisfied only for a very large pressure jump. For instance, the density jump across a strong shock with $Z = (P_2 - P_1)/P_1 \gg 1$ is

$$\frac{\rho_2}{\rho_1} = \frac{\gamma + 1}{\gamma - 1} - \frac{4\gamma}{(\gamma - 1)^2} \frac{1}{Z} + O\left(\frac{1}{Z^2}\right). \quad (45)$$

Observe that even for large Z , the first-order corrections can be significant due to the large coefficient $-4/(\gamma - 1)^2$. For instance, in a gas with $\gamma = 5/3$, this coefficient is -15 and the leading order term is 4, thus indicating that the $1/Z$ correction is small only when $Z \gg 15/4$. Another implication of a strong

main shock is the fact that the shocked material evolves on the time scale of its own sound speed, which scales as $\sqrt{P_M}$, where P_M is the main shock pressure. Instead, the relaxed profiles evolve on a slower time scale of the order of the prepulse shock sound speed, which scales as $\sim \sqrt{P_p}$. It follows that in the limit of $\sqrt{P_M/P_p} \gg 1$, one can neglect the dynamics of the relaxed profiles during the main shock propagation. In other words, one can regard the relaxed profiles as frozen in time while the main shock propagates through. Obviously, the corrections due to a finite $\sqrt{P_M/P_p}$ may be large and need to be estimated.

For the sake of simplicity, we will first proceed by neglecting the finite main shock strength correction, assume that the relaxed profiles are frozen, and determine the lowest-order solution. The finite shock strength effects will be estimated later as corrections to the lowest-order solution.

Effects of mass ablation and residual ablation pressures, though important, are also neglected in this article, and the calculation focuses on the ideal case of a strong shock supported by a constant applied pressure traveling up a relaxed density profile described by the power laws (18) or [(43), (44)].

1. Shock Propagation Through a Relaxed Profile of the First Kind

As indicated earlier in **Relaxed Profiles of the First Kind** (p. 108), the density profile generated by a rarefaction wave before its interaction with the prepulse shock is described by a simple power law of the areal density $\rho = (m/m_{\text{rf}})^\alpha$ with $\alpha = 2/(\gamma + 1) = 0.75$. Here $m_{\text{rf}} = a_p \rho_p t$ is the location of the rarefaction leading edge. If the main shock is much stronger than the prepulse shock, then the relaxed profile may be considered as frozen in time during the fast main shock propagation. Since both shocks must merge at the shell's inner surface, the fast main shock is launched when the prepulse shock is approaching the inner shell surface. One can therefore approximate $m_{\text{rf}} \approx m_{\text{shell}}$ to lowest order in the inverse shock strength.

a. The approximation of a static relaxed profile. Introducing the new variable $\zeta \equiv m/m_{\text{rf}} \approx m/m_{\text{shell}}$, the relaxed profile can be represented by the simple power law

$$\rho = \rho_p \zeta^\alpha, \quad \alpha = \frac{2}{\gamma + 1}, \quad (46)$$

with $0 < \zeta < 1$. To simplify the analysis, we introduce another dimensionless variable related to the main shock location:

$$\xi = \frac{m}{m_s^M} = \frac{\zeta}{\zeta_s^M}, \quad (47)$$

where both m_s^M and ζ_s^M represent the main shock location in their respective coordinates. Obviously, $0 < \xi < 1$ with $\xi = 1$ representing the shock position. The profiles left behind by the main shock can be written in terms of the variables ζ and ξ in the following form:

$$\rho = \frac{\rho_M \xi^\alpha}{\Phi(\xi)^{1/\gamma}}, \quad S = \frac{S_M}{\xi^{\gamma\alpha}}, \quad (48)$$

$$P = \frac{P_M}{\Phi(\xi)}, \quad u = a_M \frac{U(\xi)}{\xi^{\alpha/2}}, \quad (49)$$

where

$$\rho_M \equiv \rho_p (\gamma + 1) / (\gamma - 1),$$

$$P_M = S_M \rho_M^\gamma,$$

$$a_M \equiv \sqrt{\gamma P_M / \rho_M},$$

and $\Phi(\xi)$, $U(\xi)$, and S_M need to be determined. By inspection of Eqs. (48) and (49), it is clear that by setting $\Phi(1) = 1$, the pressure immediately behind the shock is P_M . Furthermore, using the Hugoniot condition for the post-shock velocity, one can immediately deduce that $U(1) = \sqrt{2/\gamma(\gamma-1)}$. Substituting Eqs. (48) and (49) into the equations of motion and using the Hugoniot condition for the shock velocity,

$$\dot{m}_s^M = \sqrt{\frac{\gamma-1}{2} P_M \rho_M (\zeta_s^M)^\alpha}, \quad (50)$$

it is straightforward to derive the two equations governing Φ and U :

$$\xi \sqrt{\frac{\gamma-1}{2\gamma}} \frac{d\Phi^{1/\gamma}}{d\xi} - \frac{\alpha}{2} \frac{U}{\xi^{1-(\alpha/2)}} + \xi^{\alpha/2} \frac{dU}{d\xi} = 0, \quad (51)$$

$$\sqrt{\frac{\gamma(\gamma-1)}{2}} \xi^{1-(\alpha/2)} \frac{dU}{d\xi} - \frac{d}{d\xi} \frac{1}{\Phi} = 0, \quad (52)$$

which need to be solved with the initial conditions $\Phi(1) = 1$ and $U(1) = \sqrt{2/\gamma(\gamma-1)}$. The unknown S_M can be determined by requiring that the solution of Eqs. (51) and (52) reproduces the applied pressure P_f at $m = 0$. Using Eq. (49), one finds the following expression for S_M and the pressure behind the shock P_M :

$$S_M = \frac{P_f \Phi(0)}{\rho_M^\gamma}, \quad P_M = P_f \Phi(0). \quad (53)$$

Observe that the pressure behind the shock is constant throughout the shock propagation. An approximate yet quite accurate solution of Eqs. (51) and (52) can be found by using the following ansatz:

$$\Phi(\xi) \approx \frac{\Phi(0)}{1 + \xi [\Phi(0) - 1]}. \quad (54)$$

Substituting Eq. (54) into (52) and using the boundary condition for the velocity at the shock front yields

$$U(\xi) \approx \sqrt{\frac{2}{\gamma(\gamma-1)}} \left\{ \left[1 - \frac{1}{\Phi(0)} \right] \frac{2}{\alpha} (\xi^{\alpha/2} - 1) + 1 \right\}. \quad (55)$$

The functions (54) and (55) must approximately satisfy Eq. (51), which can be rewritten upon substitution of the two functions as

$$\left[2 - \alpha - \frac{2}{\Phi(0)} \right] \frac{1}{\xi^{1-(\alpha/2)}} \approx \frac{\gamma-1}{\gamma} \frac{\Phi(0)-1}{\Phi(0)} \xi \Phi(\xi)^{(\gamma+1)/\gamma}. \quad (56)$$

Observe that since $\alpha < 2$, the left-hand side of Eq. (56) is singular for $\xi \rightarrow 0$ while the right-hand side is regular. It follows that Eq. (56) can be satisfied only when $2 - \alpha - 2/\Phi(0) \approx 0$, leading to

$$\Phi(0) \approx \frac{2}{2-\alpha} = \frac{\gamma+1}{\gamma} = 1.6. \quad (57)$$

The numerical solution of Eqs. (51) and (52) yields $\Phi(0) \approx 1.68$ in good agreement with the analytic derivation. Figure 98.47 compares the numerically derived functions $\bar{p} \equiv \Phi(0)/\Phi(\xi)$ (representing the pressure profile) and $\bar{u} \equiv U(\xi)/\xi^{\alpha/2}$ (representing the velocity profile) with the analytic solutions from Eqs. (54), (57), and (55). Observe that the pressure increases approximately linearly before the shock, while the velocity profile is approximately flat. The shock pressure is amplified about 1.6 to 1.7 times with respect to the applied pressure. This amplification is due to the slowing down of the shocked material against the shock front. The shock-front velocity decreases in time as a power law. It can be easily derived by first determining the shock trajectory in the mass coordinate through Eq. (50) and then substituting the post-shock velocity u_{ps} calculated at the shock front [Eq. (49) at $\xi = 1$ and $m = m_s^M$] into the shock relation

$$U_{\text{shock}} = [(\gamma + 1)/2]u_{ps}.$$

This leads to the following expression for the shock velocity:

$$U_{\text{shock}} = \frac{a_M \sqrt{\frac{(\gamma + 1)^2}{2\gamma(\gamma - 1)}}}{\left[\sqrt{\frac{\gamma - 1}{2\gamma}} \frac{2 - \alpha}{2} \frac{\rho_M a_M t}{m_{\text{shell}}} \right]^{\alpha/(2-\alpha)}}, \quad (58)$$

which decreases as $1/t^{0.6}$ for $\alpha = 2/(\gamma + 1) = 0.75$.

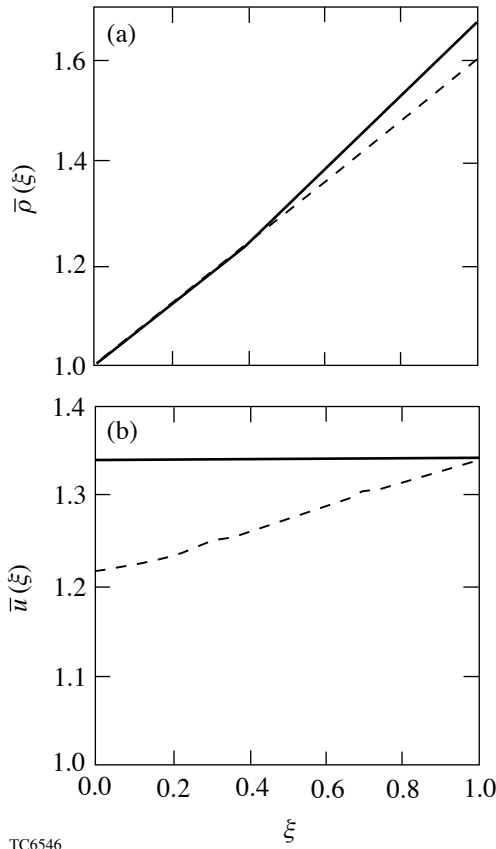
Furthermore, as indicated by Eqs. (48) and (53), the entropy profile behind the main shock follows a simple power law of the mass coordinate

$$S(m) = \frac{P_f \Phi(0)}{\rho_M^\gamma} \left(\frac{m_{\text{shell}}}{m} \right)^{\gamma\alpha}, \quad (59)$$

where the rarefaction leading edge m_{rf} has been taken near the inner surface at $m_{\text{rf}} = m_{\text{shell}}$ and $\alpha = 2/(\gamma + 1)$. Indeed, it is important to require that the main shock, the rarefaction leading edge, and the prepulse shock merge at the target's rear surface, leading to $m_{\text{rf}} \approx m_{\text{shell}} \approx m^*$. This timing requirement is discussed in the **Introduction** (p. 106), where the optimized adiabat shaping procedure is described. Figure 98.48 shows the simulated adiabat profile generated by a strong shock driven by a 26-Mbar applied pressure traveling up a relaxed target with a density profile represented by the following power law:

$$\rho = \rho_p \left[\frac{(1 - \alpha)\rho_p x}{m_{\text{shell}}} \right]^{\frac{\alpha}{1-\alpha}}, \quad (60)$$

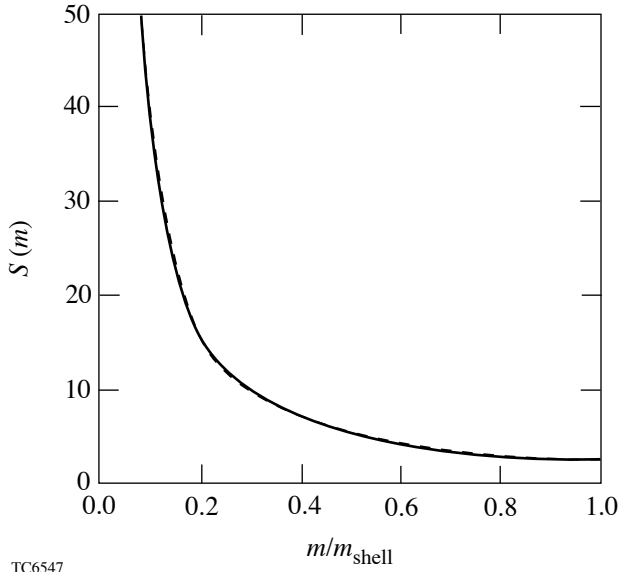
where $0 < x < m_{\text{shell}}/(1 - \alpha)\rho_p$ is the spatial coordinate. Observe that the profile in Eq. (60) requires that $\alpha < 1$ to avoid singularities at $x = 0$ (here $\alpha = 0.75$). Note Eq. (60) can be easily rewritten in terms of the mass coordinate m leading to $\rho = \rho_p (m/m_{\text{shell}})^\alpha$, which is identical to Eq. (18) with $m_{\text{rf}} = m_{\text{shell}}$. The solid curve of Fig. 98.48 represents the adiabat from the 1-D simulation, while the dashed curve is obtained from the analytic theory in Eq. (59). Observe that the two adiabat profiles are virtually identical, indicating excellent agreement between theory and simulations.



TC6546

Figure 98.47

The numerical (solid) and analytic (dashed) solutions of the self-similar (a) pressure profiles $\bar{p}(\xi)$ and (b) density profile $\bar{\rho}(\xi)$ are shown to be in relatively good agreement.



TC6547

Figure 98.48

A comparison of the simulated (solid) and analytically calculated [Eq. (59)] (dashed) adiabat shapes generated by propagating a shock supported by a constant 26-Mbar pressure through a density profile of the first kind shows excellent agreement.

b. Corrections due to dynamic relaxed profiles/finite shock strength. The analytic theory above has been derived in the limit of a relaxed profile that is stationary during the shock propagation. However, the profile varies in time as the leading edge of the rarefaction wave travels toward the shell's inner surface. Because of these changes, the resulting adiabat profile left behind by the main shock is somewhat shallower than the one predicted by Eq. (59). One can estimate the effects of dynamic profiles on the adiabat shape by assuming that the relaxed profile changes slightly over the main shock propagation interval. The dynamic corrections to the entropy profiles can be estimated by determining the entropy at the shock front located at $m_s^M(t)$:

$$S(m_s^M) = \frac{P_{ps}^M}{(\rho_{ps}^M)^\gamma}, \quad (61)$$

where P_{ps}^M and ρ_{ps}^M are the post-shock pressure and density at the main shock front, respectively. It is obvious that if one can rewrite the right-hand side of Eq. (61) as a function of the shock position, then the entropy profile is given by the RHS with m_s^M replaced by m . The post-shock density in Eq. (61) can be

rewritten in terms of the pre-shock density at the shock front ρ_{bs}^M including the linear corrections in the inverse shock strength:

$$\rho_{ps}^M \approx \frac{\gamma+1}{\gamma-1} \rho_{bs}^M \left[1 - \frac{4\gamma}{\gamma^2-1} \frac{P_p}{P_M} \left(\frac{m_s^M}{m_{shell}} \right)^{\gamma\alpha} \right], \quad (62)$$

where the post-shock pressure used to calculate the correction of order P_p/P_M has been taken equal to the zeroth-order solution P_M . Because of the large numerical coefficient $4\gamma/(\gamma^2-1)$, the first-order correction in the inverse shock strength shown in Eq. (62) needs to be retained. Another important correction is in the pre-shock density $\rho_{bs} = \rho_p (m/m_{rf})^\alpha$, which varies in time due to the evolution of the rarefaction leading edge m_{rf} , which can be written as

$$m_{rf} = m_{shell} - a_p \rho_p (\Delta t_s^M + t_f - t), \quad (63)$$

where Δt_s^M is the travel time of the main shock through the shell and t_f is the beginning time of the laser foot when the main shock is launched. Observe that the second term on the right-hand side represents the correction to m_{rf} and is small as long as the main shock is strong. This can be quantified by calculating Δt_s^M after integrating Eq. (50) and setting $m_{rf} \approx m_{shell}$ into the variable ζ . A straightforward calculation yields

$$\Delta t_s^M \approx \sqrt{\frac{2\gamma}{\gamma-1}} \frac{2}{2-\alpha} \frac{m_{shell}}{\rho_M a_M} \quad (64)$$

and $(t-t_f)/\Delta t_s^M = (m_s^M/m_{shell})^{1-\alpha/2}$. Substituting Eq. (64) into (63) leads to the following equation for the rarefaction leading edge in terms of the main shock location:

$$m_{rf} = m_{shell} \left\{ 1 - \frac{2}{2-\alpha} \sqrt{\frac{2\gamma}{\gamma-1}} \frac{P_p}{P_M} \left[1 - \left(\frac{m_s^M}{m_{shell}} \right)^{\frac{2-\alpha}{2}} \right] \right\}. \quad (65)$$

Observe that the correction to m_{rf} is of the order of $\sqrt{P_p/P_M}$ as indicated in the introduction of **Main Shock Propagation Through the Relaxed Profiles** (p. 112) and can be significant even for a strong main shock. It follows that the post-shock density used in Eq. (61) can be rewritten, including the relevant corrections, in the following form:

$$\rho_{ps}^M = \rho_M \left(\frac{m_s^M}{m_{shell}^M} \right)^\alpha \times \frac{1 - \frac{4\gamma}{\gamma^2 - 1} \frac{P_p}{P_M} \left(\frac{m_s^M}{m_{shell}^M} \right)^{\gamma\alpha}}{\left[1 - \frac{2}{2 - \alpha} \sqrt{\frac{2\gamma}{\gamma + 1} \frac{P_p}{P_M}} \left[1 - \left(\frac{m_s^M}{m_{shell}^M} \right)^{\frac{2 - \alpha}{2}} \right] \right]^\alpha}. \quad (66)$$

The next step is the calculation of the dynamic correction to the post-shock pressure in Eq. (62). While the exact calculation of such corrections can be cumbersome, a fairly good approximation can be obtained by assuming that the post-main-shock pressure profile is linear in the mass coordinate:

$$P \approx P_f \left[1 + A(t) \frac{m}{m_s^M(t)} \right], \quad (67)$$

where $A(t)$ needs to be determined. It is important to notice that in the static relaxed profile case, $A(t)$ was previously determined to be approximately constant with $A(t) \approx A_0 \approx \alpha/(2 - \alpha)$. It follows that the dynamic corrections will lead to a change in $A(t)$, which can be rewritten as a small correction to A_0 such as

$$A(t) = A_0 + \delta A(t) + \dots, \quad (68)$$

where $\delta A \ll A_0$ needs to be determined. An important dynamic correction enters the Hugoniot relations for the velocity jump across the main shock

$$u_{ps}^M = u_{bs}^M + \sqrt{\frac{2}{\gamma + 1} \frac{P_{ps}^M}{\rho_{bs}^M}}, \quad (69)$$

where u_{bs}^M is the pre-shock velocity at the shock front given by the standard rarefaction-wave solution

$$u_{bs}^M = a_p \left[\frac{\alpha}{1 - \alpha} \left(\frac{m_s^M}{m_{rf}^M} \right)^{1 - \alpha} + \sqrt{\frac{2}{\gamma(\gamma - 1)}} - \frac{2}{\gamma - 1} \right]. \quad (70)$$

Observe that u_{bs} represents a correction of the order of $\sqrt{P_p/P_M}$ in the Hugoniot relation [Eq. (69)] and can be evaluated using the lowest-order form of $m_{rf}^M \approx m_{shell}^M$. Instead, the pre-shock density $\rho_{bs}^M = \rho_b (m_s^M/m_{rf}^M)^\alpha$ in Eq. (69) needs to include the lowest-order corrections for m_{rf} given in Eq. (65). Conservation of momentum requires that the acceleration balances the pressure gradient at the shock front leading to

$$\frac{\partial u_{ps}^M}{\partial t} = - \left(\frac{\partial P}{\partial m} \right)_{m_s^M}. \quad (71)$$

Substituting Eqs. (67)–(70) into (71) yields the following ordinary differential equation for δA :

$$\frac{d}{d\eta} (\eta^{2 - \alpha} \delta A) = - \frac{2\alpha}{2 - \alpha} \sqrt{\frac{P_b}{P_M}} \times \left[\sqrt{\frac{2\gamma}{\gamma + 1}} + \sqrt{2\gamma(\gamma + 1)} \right] \eta^{2 - \frac{3\alpha}{2}}, \quad (72)$$

where $\eta \equiv m_s^M/m_{shell}^M$. Equation (72) can be integrated using the initial condition that $\delta A(m_s^M = 0) = 0$, leading to the following final form of the post-shock pressure at the shock front:

$$P_{ps}^M = P_M \left\{ 1 - \frac{2\alpha}{3(2 - \alpha)} \sqrt{\frac{P_p}{P_M}} \times \left[\sqrt{\frac{2\gamma}{\gamma + 1}} + \sqrt{2\gamma(\gamma + 1)} \right] \eta^{1 - \frac{\alpha}{2}} \right\}. \quad (73)$$

Observe that the corrections due to finite main shock strength cause the main shock pressure to decrease as the shock propagates through the dynamic relaxed profile. This clearly leads to a gentler decrease in entropy.

The last step is to substitute Eqs. (66) and (73) into (61) and derive the final form of the adiabat shape:

$$S(m) = S_{\text{in}} \left(\frac{m_{\text{shell}}}{m} \right)^{\frac{2\gamma}{\gamma+1}} \frac{\chi \left(\frac{m}{m_{\text{shell}}} \right)}{\chi(1)}, \quad (74)$$

where

$$S_{\text{in}} = c_0 \frac{(\gamma-1)^{2\gamma} \chi(1) P_f}{\gamma(\gamma+1)^{2\gamma-1} \rho_0^\gamma} \quad (75)$$

is the entropy on the inner shell surface, $c_0 = 1.68/1.6 = 1.05$ is a corrective factor to account for the analytical approximation used in Eq. (54), and ρ_0 is the initial shell density.

The function $\chi(x)$ represents the corrections due to the finite main shock strength

$$\chi(x) = \left[1 - \frac{2\sqrt{2}}{3} \frac{\gamma+2}{\gamma+1} \sqrt{\frac{P_p}{P_f}} x^{\frac{\gamma}{\gamma+1}} \right] \times \frac{\left[1 - \sqrt{\frac{2P_p}{P_f}} \left(1 - x^{\frac{\gamma}{\gamma+1}} \right) \right]^{\frac{2\gamma}{\gamma+1}}}{\left[1 - \frac{4\gamma^2}{(\gamma+1)^2(\gamma-1)} \frac{P_p}{P_f} x^{\frac{2\gamma}{\gamma+1}} \right]^\gamma}, \quad (76)$$

where the relation $\alpha = 2/(\gamma+1)$ has been used and P_p/P_f is the ratio of the prepulse pressure to the pressure of the foot of the main pulse. This concludes the analysis of the main shock propagation through a relaxed profile of the first kind. The next step is to investigate the main shock propagation through relaxed profiles of the second kind and determine the resulting adiabat shape.

2. Shock Propagation Through a Relaxed Profile of the Second Kind

In the case of a short prepulse, the rarefaction wave catches the shock at $m = m_*$ before the inner surface ($m < m_{\text{shell}}$), and the shock decays until it reaches the inner surface at $m = m_{\text{shell}}$.

As described in **Relaxed Profiles of the Second Kind** (p. 108), the relaxed profile for $\gamma = 5/3$ is well-approximated by two power laws of the mass coordinate: $\rho \sim m^{0.75}$ for $m < m_*$ and $\rho \sim m^{1.45}$ for $m_* < m < m_{\text{shell}}$. The analysis of the main shock propagation through such a profile is vastly more complicated with respect to the case of the single power-law profile discussed in **Shock Propagation Through a Relaxed Profile of the First Kind** (p. 112). An approximate analytic solution can be found, however, by assuming that the pressure profile behind the main shock is linear in the mass coordinate. Similar to the case of profiles of the first kind, we will first consider the approximation of infinite main shock strength and static relaxed profiles. The corrections due to the finite shock strength and dynamic profiles are estimated *a posteriori* as small perturbations of the zeroth-order solution.

a. The approximation of a strong shock and a static relaxed profile. In the static case, the relaxed profile in the region $m < m_*$ is identical to the profile of the first kind, leading to a pressure profile behind the shock that linearly increases about 60% with respect to the applied foot pressure P_f . Once the main shock enters into the second region $m_* < m < m_{\text{shell}}$, an exact analytic solution cannot be found. A careful analysis of the numerical simulation indicates, however, that the pressure profile behind the shock remains approximately linear in the mass coordinate. In contrast with the behavior in the first region, however, the shock-front pressure is not constant while the pressure at m_* varies slightly around the value ωP_f with $\omega \approx 1.5$ to 1.6 for $\gamma = 5/3$. Thus, it makes sense to look for a solution of the hydrodynamic equation with a linear pressure profile of the following form:

$$P_{\text{ps}}(m > m_*) \approx \omega(\gamma) P_{\text{foot}} \left[1 + D(t) \left(\frac{m}{m_*} - 1 \right) \right], \quad (77)$$

where $\omega(\gamma)$ is a constant that must be chosen to reproduce the pressure at the time when the main shock reaches m_* . Using the results of the previous section for the main shock propagation for $m < m_*$, one can conclude that

$$\omega(\gamma) \approx \frac{\gamma+1}{\gamma}. \quad (78)$$

Similar to the analysis in **Shock Propagation Through a Relaxed Profile of the First Kind** (p. 112), Eq. (77) can be substituted into the momentum equation at the shock front $\left[\partial_t u_{\text{ps}} = -(\partial_m P) \right]_{m_*^M}$, where the post-shock velocity at the

shock front is given by the Hugoniot relation

$$u_{ps}^M = \sqrt{2P_{ps}^M / (\gamma + 1)\rho_{bs}^M}$$

with the pre-shock density at the shock front given by

$$\rho_{bs}^M = \rho_p \left(\frac{m_s^M}{m_{shell}} \right)^\mu, \quad (79)$$

where the prepulse shock location m_{sh}^p has been assumed to have reached the inner shell surface so that $m_s^p \approx m_{shell}$. As in **Shock Propagation Through a Relaxed Profile of the First Kind** (p. 112), u_{ps}^M and P_{ps}^M represent the post-shock velocity and pressure at the main shock front. The resulting shock-front momentum equation can be simplified by using the main shock trajectory $m_s^M(t)$ as the time coordinate and by using the shock mass velocity $\dot{m}_s^M = \sqrt{(\gamma + 1)P_{ps}^M \rho_{bs}^M} / 2$. A straightforward manipulation of the momentum equation leads to the following simple differential equation for D :

$$\frac{dD}{dz_s^M} (z_s^M - 1) + 3D - \frac{\mu}{z_s^M} \left[1 + D(z_s^M - 1) \right] = 0, \quad (80)$$

where $D = D[z_s^M]$ and $z_s^M \equiv m_s^M(t)/m_*$. It is important to note that the only nonsingular solution of Eq. (80) has the simple form

$$D(x) = \frac{2(x^\mu - 1) + \mu(x - 3)(x - 1) - \mu^2(x - 1)^2}{(\mu - 2)(\mu - 1)(x - 1)^3}. \quad (81)$$

The pressure at the shock fronts can be determined from Eq. (77) upon substitution of Eq. (81), leading to

$$P_{ps}^M(m_s^M) \approx \omega(\gamma)P_f \left[1 + D\left(\frac{m_s^M}{m_*}\right) \left(\frac{m_s^M}{m_*} - 1\right) \right], \quad (82)$$

representing a growing function of m_s^M reaching the asymptotic value of 3.6 for $m_s^M \gg m_*$. The entropy behind the shock can be easily calculated by substituting the pressure and density at the shock front into the definition of the entropy:

$$S(m_s^M) = \frac{P_{ps}^M(m_s^M)}{\left[\rho_{ps}^M(m_s^M) \right]^\gamma}. \quad (83)$$

Using Eqs. (77), (81), and (82) into (83) leads to the following form of the entropy:

$$S_\infty(m_* < m \leq m_{shell}) = \frac{\omega(\gamma)P_f}{\rho_M^\gamma} \times \left(\frac{m_{shell}}{m} \right)^{\gamma\mu} \left[1 + D\left(\frac{m}{m_*}\right) \left(\frac{m}{m_*} - 1\right) \right], \quad (84)$$

where $\rho_M = \rho_p(\gamma + 1)/(\gamma - 1)$ and the subscript ∞ indicates that Eq. (84) is valid only for infinite main shock strength. Figure 98.49 shows a comparison of the predicted adiabat profile of Eq. (84) (dashed) with the simulated adiabat profile (solid) generated by a strong shock driven by a 26-Mbar applied pressure traveling up a static, relaxed target with a density profile given by $\rho = \rho_M(m_*/m_{shell})^\mu(m/m_*)^\alpha$ for $m \leq m_*$, and $\rho = \rho_M(m/m_{shell})^\mu$ for $m_* < m \leq m_{shell}$. Here, m_*/m_{shell} is chosen to be 0.05. The theory again shows excellent agreement with the simulation.

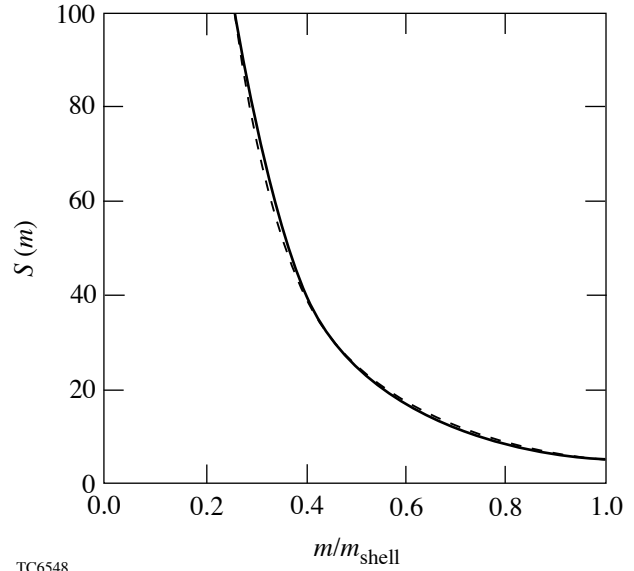


Figure 98.49

A comparison of the simulated (solid) and analytically calculated [Eq. (84)] (dashed) adiabat shape generated by propagating a shock supported by a constant 26-Mbar pressure through a density profile of the second kind shows excellent agreement.

It is interesting to observe that the linear approximation for the pressure profile leads to a flat velocity profile as shown by substituting Eq. (77) into the momentum equation, yielding

$$u(m, t) = u_{ps}^M(t). \quad (85)$$

The density behind the shock can be determined from the pressure and the entropy through the relation $\rho = (p/S)^{1/\gamma}$. Upon substitution of the density, the mass conservation equation [Eq. (4)] can be solved for the velocity profile, leading to

$$u(m, t) = u_{ps}^M \left[1 - G\left(z, z_s^M\right) \right], \quad (86)$$

where $z = m/m_*$ and

$$G\left(z, z_s^M\right) = \frac{\gamma - 1}{2\gamma} \frac{dD\left(z_s^M\right)}{dz_s^M} \times \int_{z_s^M}^z \frac{(x-1) \left[1 + D(x)(x-1) \right]^{1/\gamma} \left(\frac{z_s^M}{x} \right)^\mu}{\left[1 + D\left(z_s^M\right)(x-1) \right]^{(\gamma+1)/\gamma} \left(\frac{z_s^M}{x} \right)} dx. \quad (87)$$

Observe that the two velocity profiles obtained from the momentum and mass conservation equations are approximately equal in magnitude as long as $|G| \ll 1$. The value G can be estimated after replacing z with ηz_s^M and by plotting $G(\eta z_s^M, z_s^M)$ for $1/z_s^M < \eta < 1$ for different values of z_s^M . Figure 98.50 shows the value of G for $z_s^M = 2, 5, 10, 20$, indicating that G does not exceed 0.21 for typical values of $z_s^M \leq 20$. It follows that the linear pressure profile of Eq. (77), the flat velocity profile of Eq. (85), and the entropy profile of Eq. (84) are accurate approximations of the solution to the hydro equations.

b. Corrections due to dynamic relaxed profiles/finite shock strength. To determine the correction to the adiabat shape due to the finite shock strength and the dynamic evolution of the relaxed profile during the main shock propagation, one needs to calculate the main shock position in terms of the prepulse shock location. Both the main shock m_s^M and the prepulse shock positions m_s^P are governed by the Hugoniot relations

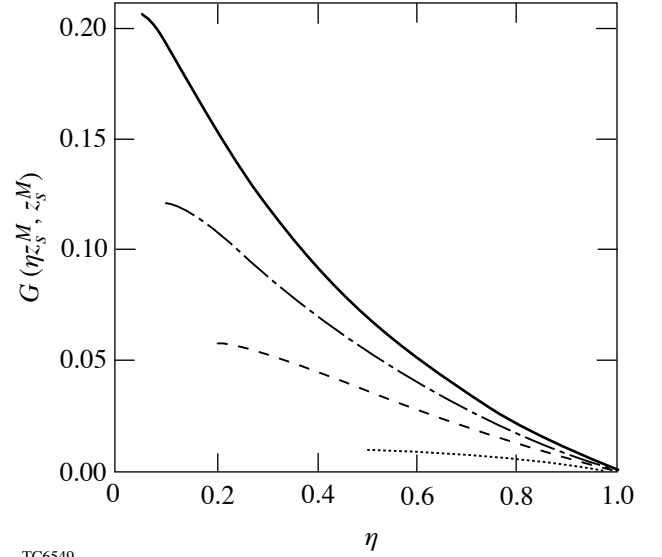


Figure 98.50
Plots of $G(\eta z_s^M, z_s^M)$ for $z_s^M = 2, 5, 10, 20$ (dotted, dashed, dash-dotted, and solid lines, respectively) show that G does not exceed 0.21 for typical values of $z_s^M \leq 20$.

$$\dot{m}_s^M = \sqrt{\frac{\gamma - 1}{2} P_f \rho_M \left(\frac{m_s^M}{m_s^P} \right)^\mu \left[1 + D\left(z_s^M\right) \left(z_s^M - 1 \right) \right]}, \quad (88)$$

$$\dot{m}_s^P = \sqrt{\frac{\gamma - 1}{2} P_p \rho_p \left(\frac{m_*}{m_s^P} \right)^\delta}, \quad (89)$$

where $\delta \approx 1.315$. Replacing the time variable with $m_s^P(t)$ into Eq. (88) leads to the following algebraic equation relating the main and the prepulse shock location:

$$\left(z_s^P \right)^\beta - z_{\text{shell}}^\beta = \beta \sqrt{\frac{2(\gamma - 1)}{\gamma + 1} \frac{P_p}{\omega(\gamma) P_f}} \times \left[\sigma\left(z_s^M\right) - \sigma\left(z_{\text{shell}}\right) \right], \quad (90)$$

where $\beta = (\delta - \mu + 2)/2$, $z_s^P = m_s^P/m_*$, $z_{\text{shell}} = m_{\text{shell}}/m_*$, and

$$\sigma(\xi) = \sqrt{\frac{(\mu-2)\xi^{1-\mu} - (\mu-1)\xi^{2-\mu} + 1}{(\mu-2)(\mu-1)}}. \quad (91)$$

It is important to recognize that Eq. (90) has been derived using the condition that $z_s^P = z_{\text{shell}}^P$ when $z_s^M = z_{\text{shell}}^M$. This is an essential constraint requiring that both the prepulse and main shock merge on the shell's inner surface. Observe that Eq. (90) can be used to find z_s^P in terms of z_s^M . An analytic form of z_s^M in terms of z_s^P can also be found by approximating $\mu \approx 1.45$ and reducing Eq. (90) to a second-order algebraic equation for z_s^M .

Similar to the analysis in **Shock Propagation Through a Relaxed Profile of the First Kind** (p. 112), we estimate the dynamic corrections to the entropy profile by rewriting the entropy at the main shock front:

$$S(z_s^M) = \left(\frac{z_s^P}{z_s^M}\right)^{\mu\gamma} \frac{P_{\text{ps}}^M(z_s^M, t)}{\rho_M^\gamma}. \quad (92)$$

Since we did not find an exact solution of the post-shock pressure for the static case, it is not worth calculating small corrections to an already inexact solution. Nevertheless, we retain the corrections due to the dynamic evolution of the relaxed profile. These corrections require including the time dependence of z_s^P in the pre-shock density. We speculate that the largest corrections to the entropy are likely to come from such dynamic effects. This consideration is supported by the large power index $\mu\gamma \approx 2.4$ for z_s^P in Eq. (92) and the finite shock strength corrections of the order of $\sqrt{P_p/P_f}$ in Eq. (92) for z_s^P . It follows that the dynamic corrections to the entropy profile can be determined by substituting z_s^P from Eq. (90) into Eq. (92) and by replacing z_s^M with $z = m/m_*$. A straightforward manipulation leads to the following form of the entropy profile:

$$S(m) = S_\infty(m) \left\{ 1 - \beta \left(\frac{m_*}{m_{\text{shell}}}\right)^\beta \sqrt{\frac{2(\gamma-1)}{(\gamma+1)} \frac{P_p}{P_f}} \right. \\ \left. \times \left[\sigma\left(\frac{m_{\text{shell}}}{m_*}\right) - \sigma\left(\frac{m}{m_*}\right) \right] \right\}^{\frac{\gamma\mu}{\beta}}, \quad (93)$$

where S_∞ is given in Eq. (84). Observe that dynamic corrections to the adiabat shape lead to a shallower profile.

Conclusion

We have derived analytical forms of the relaxation adiabat shapes for (1) the case where the prepulse is long enough that the rarefaction wave catches the prepulse shock at the rear surface of the shell, and (2) the case of short prepulses, where the mass undertaken by the unattenuated prepulse shock is less than the total mass of the shell. The analytic relaxation adiabat profiles derived here are in excellent agreement with simulation. In addition, we have shown that relaxation designs with short prepulses lead to steeper adiabat gradients than decaying shock designs. The effects of mass ablation and residual ablation pressure on relaxation adiabat shapes will be analyzed in a future article.

ACKNOWLEDGMENT

This work was supported by the U.S. Department of Energy Office of Inertial Confinement Fusion under Cooperative Agreement No. DE-FC03-92SF19460, the University of Rochester, and the New York State Energy Research and Development Authority. The support of DOE does not constitute an endorsement by DOE of the views expressed in this article.

Appendix A: Relaxed Density Profiles in Real Space

A better understanding of the relaxed profile shape can be obtained by converting the profile functions from the Lagrangian coordinate m to the spatial coordinate x . Equation (3) relating the mass to the initial density is also valid if the initial density is replaced by the density at time t as long as the lower limit and upper limit of integration are the trajectory of the outer surface $x_{\text{out}}(t)$ and the trajectory of generic fluid element $x(t)$. It follows that the conversion between mass and real space is straightforward once the relation between m and x is rewritten in the differential form

$$\frac{dm}{dx} = \rho(x, t). \quad (A1)$$

Equation (A1) is then used to rewrite the profiles of the first kind [Eq. (18)] and second kind [Eqs. (43) and (44)] in real space.

1. Relaxed Profiles of the First Kind

In the case where the shock and rarefaction merge at the inner shell surface, one can substitute Eq. (A1) into (18) and find the density profile shape in real space:

$$\rho = \rho_p \left[\frac{\gamma-1}{\gamma+1} \frac{x - x_{\text{out}}}{a_p t} \right]^{\frac{2}{\gamma-1}}, \quad (A2)$$

where x_{out} is the trajectory of the outer shell surface coinciding with the trailing edge of the rarefaction wave moving away from the shell with the escape velocity $2a_p/(\gamma - 1)$. The range of x in Eq. (A2) is limited by the trailing and leading edge of the rarefaction wave. Since the leading edge travels inside the shell with the sound speed, the range of x is limited by $x_{\text{out}} < x < x_{\text{out}} + a_p t$. Note that $t = 0$ at the time when the prepulse ends and the rarefaction is launched. Equation (A2) indicates that, in real space, the density profile is a simple power law of the distance from the rarefaction trailing edge. The leading edge of the rarefaction wave reaches the prepulse shock at the inner shell surface ($m_* = m_{\text{shell}}$) at the time

$$t_{\text{shell}} = \frac{m_{\text{shell}}}{(a_p \rho_p)} = \frac{\gamma - 1}{\gamma + 1} \frac{d_{\text{shell}}}{a_p}, \quad (\text{A3})$$

where d_{shell} is the initial shell thickness and $m_{\text{shell}} = \rho_0 d_{\text{shell}}$ is the total shell mass. At this time, the density profile is simply

$$\rho(t = t_{\text{shell}}) = \rho_p \left(\frac{x - x_{\text{out}}}{d_{\text{shell}}} \right)^{\frac{2}{\gamma - 1}}. \quad (\text{A4})$$

Note that the profile extends over a distance equal to the uncompressed shell thickness d_{shell} and approaches the compressed density ρ_p on the shell's inner surface located at $x_{\text{in}} = x_{\text{out}} + d_{\text{shell}}$.

2. Relaxed Profiles of the Second Kind

By defining with $x_*(\tau)$ the trajectory of the Lagrangian point corresponding to the fluid element where the prepulse shock and rarefaction wave interact (i.e., $m = m_*$), and with $x_s^p(\tau)$ the location of the prepulse shock after the interaction, the spatial density profile for the region $x_*(\tau) < x < x_s^p(\tau)$ can be obtained by substituting Eq. (A1) into Eq. (44), leading to

$$\rho = \rho_p \left[\frac{1}{1 + 4(\mu - 1) \left(1 - x/x_s^p\right)} \right]^{\frac{\mu}{\mu - 1}}, \quad (\text{A5})$$

where $\mu = 1.45$ for $\gamma = 5/3$. By defining with $\bar{x}_* \equiv x_*(1)$ the initial position inside the shell of the shock–rarefaction interaction point, it is straightforward to show that

$$x_s^p(\tau) = \bar{x}_* z_s^p(\tau), \quad (\text{A6})$$

$$x_*(\tau) = \bar{x}_* z_s^p(\tau) \left[1 + \frac{1 - z_s^p(\tau)}{4(\mu - 1)} \right], \quad (\text{A7})$$

where z_s^p is given in Eq. (31). Equation (A5) represents the spatial density profile of the shell portion between the shock–rarefaction merging point and the shock front. The density profile of the remaining portion between the shock–rarefaction merging point and the outer shell surface is described by Eq. (43) and in real space can again be determined by integrating Eq. (43) upon substitution of Eq. (A1). The result is similar to the density profile of the first kind and yields

$$\rho = \rho_p \left(\frac{\gamma - 1}{\gamma + 1} \frac{x - x_{\text{out}}}{a_p t} \right)^{\frac{2}{\gamma - 1}}. \quad (\text{A8})$$

It is important to emphasize that the density profiles [Eqs. (43) and (44)] are approximate solutions; therefore, the profiles [Eqs. (A5) and (A8)] are also approximate solutions. The location of the rarefaction trailing edge (or outer shell surface) cannot be exactly calculated because it is affected by the sound waves traveling down from the point of shock–rarefaction interaction. An approximate form of x_{out} can be derived by requiring that the density is continuous at $x = x_*(\tau)$, thus setting Eq. (A8) equal to Eq. (A5) at $x_*(\tau)$. This leads to the following form of x_{out} :

$$x_{\text{out}} = x_*(\tau) - \bar{x}_* \frac{a_p \tau}{z_s^p(\tau) \frac{\mu(\gamma - 1)}{2}}. \quad (\text{A9})$$

Observe that, in real space, the density profile is represented by two very different functions of x : Eq. (A5) describes the profile behind the shock, and Eq. (A8) describes the profile behind the rarefaction–shock merging point.

REFERENCES

1. K. Anderson and R. Betti, *Phys. Plasmas* **10**, 4448 (2003).
2. V. N. Goncharov, J. P. Knauer, P. W. McKenty, P. B. Radha, T. C. Sangster, S. Skupsky, R. Betti, R. L. McCrory, and D. D. Meyerhofer, *Phys. Plasmas* **10**, 1906 (2003).
3. K. Anderson and R. Betti, *Phys. Plasmas* **11**, 5 (2004).